2021-07-27

Use of Vertical Electrical Impedance for Nondestructive Evaluation of Concrete Bridge Decks

Enoch Thomas Boekweg
Brigham Young University

Use of Vertical Electrical Impedance for Nondestructive Evaluation of Concrete Bridge Decks

Enoch Thomas Boekweg

A thesis submitted to the faculty of
Brigham Young University
in partial fulfillment of the requirements for the degree of

Master of Science

Brian Mazzeo, Chair
W. Spencer Guthrie
Stephen Schultz

Department of Electrical and Computer Engineering

Brigham Young University

ABSTRACT

Use of Vertical Electrical Impedance for Nondestructive Evaluation of Concrete Bridge Decks

Enoch Thomas Boekweg
Department of Electrical and Computer Engineering, BYU
Master of Science

Nondestructive evaluation of civil infrastructure is increasingly important in the modern world to assess structures, predict longevity, and prescribe rehabilitation or replacement. For concrete bridge decks, one emerging diagnostic technique is vertical electrical impedance (VEI) testing, which is a nondestructive evaluation technology that quantitatively assesses the cover protection offered to steel reinforcement. Because VEI testing is still a relatively new approach to bridge deck inspection, additional studies are needed to increase the interpretability of VEI data. This thesis increases VEI interpretability with two advances. The first advance, presented in Chapter 2, offers an analytical model for interpreting VEI measurements of cracked bridge decks. The analytical model allows crack depth to be predicted from VEI measurements. The second advance, presented in Chapter 3, offers an interpretation of VEI measurements within the context of other, more typical, nondestructive bridge deck measurements.

Surface cracks cause a significant acceleration of chloride ingress towards the steel reinforcement because they provide a direct path for chlorides to penetrate the concrete cover and corrode the steel. Estimating the depth of these cracks enables better prediction of chloride loading and influences predictions of service life. An invertible analytical model for VEI measurements of cracks based on a cylindrical dipole approximation is presented. This model is validated with numerical simulations, laboratory experiments, and destructive field tests performed on concrete parking garage decks. Inversion of the model permits depth estimation of cracks and a quantitative interpretation of VEI measurements for this specific concrete defect.

An additional study was performed on a newly constructed bridge deck in Midvale, Utah, that was subject to an unexpected rainstorm during construction. Several forms of nondestructive testing, including VEI testing, were performed on the deck. Statistical analysis of the tests permitted assessment of the bridge deck. Comparing VEI testing with these other NDT methods has not been done before, and the results of this work will assist those who are unfamiliar with VEI with interpretation of VEI data in the context of other, more typical NDT techniques.

Keywords: bridge deck, concrete, nondestructive evaluation, vertical electrical impedance

ACKNOWLEDGEMENTS

I am extremely grateful for my wife Stephanie's tremendous support, encouragement, and belief in me. Her willingness to regularly sacrifice evening and weekend plans so that I could study and write are very appreciated. She has read my papers and thesis and helped with edits, grammar, citation formatting, and more. She is practically the fourth member of my graduate committee. A huge thanks to her! I love you, Steph!

I am also profoundly grateful for Dr. Mazzeo and Dr. Guthrie. I have been working with both for years as they have invested much of their time and resources to help me succeed as a student. Dr. Mazzeo took me under his wing years ago when he hired me to work in his research group. He has invested absurd amounts of time into mentoring me. He has shown me, through example, to pray to Heavenly Father for help in solving difficult problems, and he has always given me opportunities to work on difficult problems. His confidence that I would swim when thrown into the deep end has helped me become a better, albeit, semi-drowned, swimmer. I am also grateful for the mentorship from Dr. Guthrie. I am grateful for the many long days, and sometimes nights, that I spent on field tests with him and his students. His preparation and structure taught me a lot.

I also thank my parents. They were the first to support and encourage me in my early days of engineering studies. I am very thankful that they were always there to support and believe in me through the long and hard semesters.

I also acknowledge funding support from UDOT and ACI, as well as assistance from Robert Dayley and Terry Holt in cutting concrete samples.

TABLE OF CONTENTS

LIST OF TABLES

LIST OF FIGURES

CHAPTER 1. INTRODUCTION

1.1 Problem Statement

In transportation networks, concrete bridge decks are critical components. Of all the components of the bridge, bridge decks usually deteriorate fastest and, due to traffic, are also the most difficult to inspect [1]. Keeping concrete bridge decks in good condition is critical to maintaining a robust transportation network [2]. However, maintaining bridge decks has proven to be a difficult and expensive endeavor. In 2021, 5.5% (11,125) of U.S. bridge decks were reported as needing rehabilitation or replacement. This is equivalent to 21.4 million square meters of bridge deck area being structurally deficient [3, 4].

Meeting the demands of bridge deck upkeep would be more achievable with improved bridge deck diagnostic techniques. One emerging diagnostic technique is vertical electrical impedance (VEI) testing. VEI testing is a nondestructive evaluation technology that quantitatively assesses the cover protection offered to steel reinforcement. Because VEI testing is still a relatively new approach to bridge deck inspection, additional studies are needed to increase the interpretability of VEI data.

This thesis increases VEI interpretability with two advances. The first advance, presented in Chapter 2, offers an analytical model for interpreting VEI measurements of cracked bridge decks. The analytical model allows crack depth to be predicted from VEI measurements. The second advance, presented in Chapter 3, offers an interpretation of VEI measurements within the

context of other, more typical, nondestructive bridge deck measurements. This will help individuals unacquainted with VEI to contextualize VEI measurements in terms of nondestructive testing (NDT) results more familiar to them. Both advances are novel to the study of VEI and will greatly aid in useful interpretation of VEI measurements of bridge decks.

1.2 Bridge Deck Deterioration

The bridge deck is the surface over which vehicles travel and is supported by beams and/or girders. Bridge deck concrete is densely reinforced with steel due to the heavy traffic loads a bridge deck must support.

Bridge decks are susceptible to many types of deterioration, such as cracking, concrete degradation due to adverse reactions, and corrosion of steel reinforcement [1]. Bridge decks in cold regions and coastal regions are particularly susceptible to steel corrosion due to the ingress, diffusion, and accumulation of chlorides from de-icing salts and marine salt water [1, 5-13].

Reinforcing steel corrosion is particularly hazardous for bridge decks because corroding steel expands in volume. This expansion causes significant tensile stresses in the surrounding concrete [14, 15]. Because concrete has susceptibility to tensile forces, continuing corrosion of the reinforcing steel typically leads to horizontal cracking known as delamination. Left untreated, the delamination will increase in size and severity, the cracking will reach the deck surface, concrete spalling will occur, and a pothole will form.

While preventative maintenance, including seals and overlays, can be applied during the early service life of a bridge to prevent chloride ingress, once the damage has accelerated to the point that the rebar undergoes active corrosion, expensive bridge deck rehabilitation or replacement is often necessary. For this reason, effective bridge deck management requires

evaluation of the susceptibility of a deck to steel corrosion and application of an appropriate preventative maintenance treatment before damage occurs [16]. Many techniques are available to evaluate the susceptibility of a deck to steel corrosion and to identify regions of concrete that allow for fast transport of chloride ions from the surface of the concrete to the reinforcing steel.

1.3 Destructive Bridge Deck Testing and Evaluation Techniques

Testing and evaluation techniques are separated into two categories: destructive and nondestructive. Some types of destructive tests performed on bridge decks include chloride concentration determination and coring.

1.3.1 Chloride Concentration Determination

Chloride concentration determination involves grinding concrete sampled from varying depths within the bridge deck into powder and measuring the chloride concentration of the powder in the laboratory using titration. The main purpose of this measurement is to assess if and by how much the chloride concentration has exceeded a level at which corrosion of steel is initiated (about 1.2 kg of chloride per cubic meter of concrete) [17].

1.3.2 Coring

Coring employs a circular coring bit to cut a cylindrical sample directly out of the bridge deck. Fig. 1 shows a concrete sample extracted via coring. Simple visual inspection of these cores yields valuable information about the condition of the deck. Further testing, such as petrographic analysis or rapid chloride permeability or compressive tests, can be performed on the core in the laboratory [18].

Figure 1: Core sample cut from reinforced deck

1.4 Nondestructive Bridge Deck Testing and Evaluation Techniques

Nondestructive testing techniques are generally preferred over destructive ones because they are typically faster and less expensive and leave the bridge deck intact. Nondestructive tests commonly performed on bridge decks include visual inspection, chain dragging and hammer sounding, half-cell potential testing, resistivity testing, infrared thermography, ground penetrating radar, and VEI testing. Many of these techniques may be automated or performed from moving platforms.

1.4.1 Visual Inspection

Visual inspection is the most common nondestructive test and is typically the first step in bridge deck condition assessment [1]. Visual inspection can entail general scanning of the bridge deck for large defects such as potholes, or it can entail more focused inspection, such as creating detailed crack maps. Depending on the level of detail needed, visual inspection may also require

lane closures. When humans assess distress, there is inevitable subjectivity in the evaluation results.

1.4.2 Chain Dragging and Hammer Sounding

Chain dragging involves an inspector pulling a heavy chain or tool consisting of an arrangement of chains across the surface of a bridge deck and listening for changes in the acoustic response. Delaminations, which are invisible to the naked eye, alter the acoustic response. The inspector repeatedly passes the chain over acoustic anomalies to determine the perimeter of possible delaminations. While widely practiced, chain dragging is limited by subjectivity. Since differences in acoustic responses are dependent on the hearing ability of the inspector, achieving high repeatability is difficult [18]. Hammer or rod sounding may also be used. Impacting the surface excites flexural modes that are audible, revealing subsurface delaminations. Automated versions of these types of tests can now be performed at high speeds [19].

1.4.3 Half-Cell Potential Testing

Half-cell potential estimates the probability that the steel reinforcement is undergoing active corrosion. This test is performed by measuring the half-cell potential between a copper electrode positioned on the deck surface and the reinforcing steel, which is usually accessed through a small hole drilled into the deck (thus making this a slightly destructive test). As the corrosion activity increases, the measured half-cell potential decreases [20].

1.4.4 Resistivity Testing

Resistivity testing involves placing small probes on the surface of the concrete to measure the electrical resistance across a horizontal section of concrete cover. These resistivity measurements are correlated with the ionic diffusivity of the surface concrete and so are dependent on the concrete network of interconnected pores but also on the presence of conductive ions, typically chlorides. These measurements are taken to indicate the likelihood of reinforcing steel to corrode [21]. Notably, under typical testing configurations, these tests only interrogate a shallow depth of concrete in a direction parallel to the deck surface.

1.4.5 Infrared Thermography

Infrared thermography involves measuring temperature differentials on the surface of a concrete bridge deck. This technique exploits the fact that delaminated or damaged sections of a bridge deck will heat or cool faster than adjacent, intact sections of a bridge deck. Therefore, infrared thermography can be useful in detecting delamination [22]. Because a thermal camera does not need long exposure times, it can also be performed by ground or aerial vehicles with suitable equipment. However, infrared thermography is dependent on ambient conditions, which can affect the interpretability of measurements.

1.4.6 Ground Penetrating Radar

As the name suggests, ground penetrating radar works by transmitting electromagnetic energy into the bridge deck and then measuring the time response and energy of reflected waves returning to the receiver. Differences in reflection time often indicate regions in the concrete where changes in dielectric value occur, with metals such as steel being readily detectable. This technique is often used to create a map of the attenuation and reflection depth properties over the

measured region. Rebar location and depth, occurrence of delamination, and chloride concentration can be estimated from such maps [23].

1.5 Vertical Electrical Impedance Testing

VEI testing is used to measure the impedance of a bridge deck vertically from the deck surface down to the reinforcing steel. VEI quantifies how well the concrete cover is protecting the reinforcing steel from chloride ingress. These measurements can detect cracks, delamination, high concrete porosity, high chloride concentration, and any other factor that would result in a lower impedance, indicating a potentially faster transport of chloride ions toward the reinforcing steel. A guarded probe confines the electrical current to the concrete volume directly underneath the probe. A current return path from the guarded probe through the steel reinforcement to the apparatus is necessary to complete the electrical circuit.

This technique is relatively new, with development beginning at Brigham Young University in 2010 and an initial 2012 study concluding that VEI could assess the susceptibility of reinforcing steel to corrosion on bare concrete decks [24]. In 2015, a similar study concluded that VEI could also measure susceptibility through asphalt overlays [8]. With knowledge that VEI could assess the susceptibility of concrete cover to chloride ingress, researchers began development of equipment that could quickly and accurately measure VEI over large deck areas. A 2018 study reported a design for a rolling probe that could rapidly scan VEI in motion [25]. The limitation of this arrangement was that it required a tapped connection directly to the reinforcing steel. Fig. 2 shows how a direct tap is configured to allow impedance measurements from the surface of the deck to the steel reinforcement.

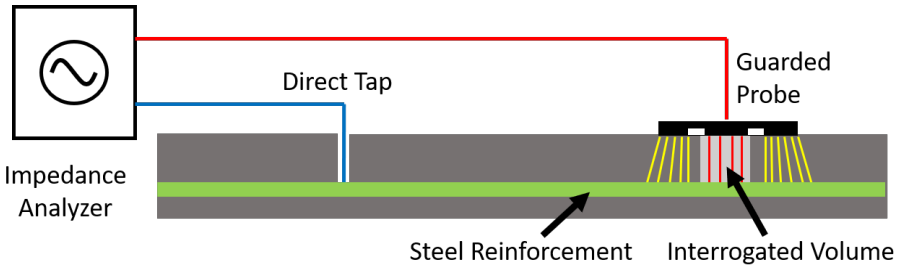

Figure 2: Vertical electrical impedance measurement employing a guarded probe and direct rebar tap.

A follow-up study published in 2019 overcame this issue by reporting the development of a device that could measure VEI without a direct tap to the reinforcing steel, thereby making the entire measurement fast, mobile, and completely nondestructive [26]. Fig. 3 shows the implementation of a large-area electrode (LAE) to overcome the need for a direct tap to the reinforcing steel by forming a low-impedance connection to the steel reinforcement.

Further development was demonstrated in 2020 with a paper detailing a multi-channel VEI device [27]. This device enabled rapid VEI measurements across a full lane width and is currently the state-of-the-art for VEI measurements of concrete bridge decks. Fig. 4 shows the multi-channel VEI measurement device in an active test of a bridge deck.

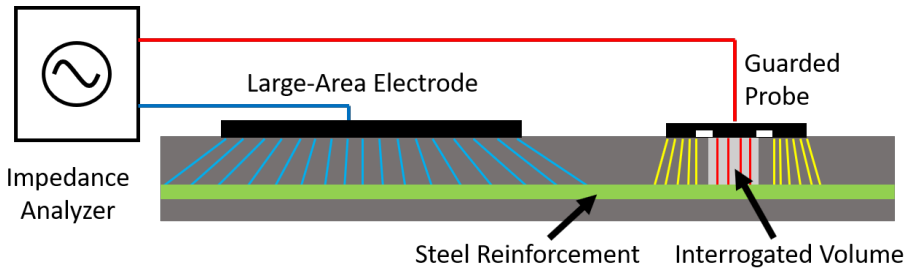

Figure 3: Vertical electrical impedance measurement employing a guarded probe and large-area electrode.

Figure 4: Multichannel VEI measurement device.

1.6 Publications

A number of publications were authored during the execution of this research. They include the following:

1. E. Boekweg, W. S. Guthrie, and B. A. Mazzeo, "Reinforced Concrete Crack Depth Estimation by Vertical Electrical Impedance," To be submitted, 2021.

2. E. Boekweg, W. S. Guthrie, and B. A. Mazzeo, "Nondestructive Evaluation of a New Concrete Bridge Deck Subject to Excessive Rainfall during Construction: Implications for Durability in a Cold Region," *2021 Regional Conference on Permafrost and 19th*

International Conference on Cold Region Engineering, American Society of Civil Engineers, 2021.

3. L. Hendricks, J. Baxter, Y. Chou, M. Thomas, E. Boekweg, W. S. Guthrie, and B. A. Mazzeo, "High-Speed Acoustic Impact-Echo Sounding of Concrete Bridge Decks," *Journal of Nondestructive Evaluation* 39:58, 2020.

1.7 Overview of Thesis

This thesis comprises three additional chapters. Chapter 2 addresses the use of VEI data for estimating concrete crack depth. Surface cracks in concrete are visible signs of deterioration that represent distressed areas where deterioration can accelerate, but crack depth is not visually discernable. While VEI testing can determine the level of protection that concrete cover offers steel reinforcement and has been used to localize cover defects, a need exists to quantitatively interpret VEI measurements in terms of specific defect characteristics such as cracks. This work quantitatively addresses interpretation of VEI measurements obtained on concrete having vertical cracks. An invertible analytical model for VEI measurements of cracks based on a cylindrical dipole approximation is presented. This model is validated with numerical simulations, laboratory experiments, and destructive field tests performed on concrete parking garage decks. Inversion of the model permits depth estimation of cracks and a quantitative interpretation of VEI measurements for this specific concrete defect.

Chapter 3 demonstrates an application of VEI testing in a series of nondestructive evaluation techniques for quality assurance of a newly constructed bridge deck in northern Utah that was subjected to an unexpected rainstorm during concrete placement. Because excess water can lead to lower concrete durability, evaluating the ability of water and chloride ions to

penetrate the concrete and quantifying the overall protection of the reinforcing steel were important objectives. Several deck properties were measured, including concrete cover depth, deck surface temperature, resistivity, VEI, and Schmidt rebound number. Statistical analyses performed on the collected data indicated that the section most affected by the rain exhibited a lower Schmidt rebound number but was not different from the other sections in terms of resistivity or VEI; therefore, the results of the testing suggest that the effect of the rain was limited to a shallow depth of concrete, which was corroborated by petrographic analysis performed on several cores removed from the bridge deck.

Chapter 4 offers a summary of the research described in Chapters 2 and 3 and explains how this work contributes to the interpretability of VEI measurements. Chapter 4 then discusses additional research that is recommended to extend the present work and establishes the importance of increased interpretability of VEI measurements for concrete bridge deck management.

CHAPTER 2. USE OF VERTICAL ELECTRICAL IMPEDANCE MEASUREMENTS FOR ESTIMATING CRACK DEPTH IN REINFORCED CONCRETE

2.0 Introduction

In transportation networks, concrete bridge decks are critical components. Of all the components of the bridge, bridge decks usually deteriorate fastest and, due to traffic, are also the most difficult to inspect [1]. Keeping concrete bridge decks in good condition is critical to maintaining a robust transportation network [2]. However, maintaining bridge decks has proven to be a difficult and expensive endeavor. In 2021, 5.5% (11,125) of U.S. bridge decks were reported as needing rehabilitation or replacement. This is equivalent to 21.4 million square meters of bridge deck area being structurally deficient [3, 4].

The process of chloride ingress into concrete bridge decks, chloride accumulation in the vicinity of steel reinforcement, and subsequent corrosion is a primary deterioration mechanism, especially in cold regions, where salt is applied to enhance safety, and in coastal regions. The primary defense against chloride-induced corrosion of the reinforcing steel is the concrete cover, or the layer of concrete that covers the top mat of rebar. When intact, this layer of concrete impedes the movement of chlorides toward the steel reinforcement. However, vertical cracks in the concrete cover are direct pathways for chloride ingress between the concrete surface and the

steel reinforcement. Quantifying concrete cover integrity is essential for identifying weaknesses in the cover protection and for planning effective maintenance and rehabilitation.

VEI measurements are well-suited for quantifying the integrity of the concrete cover [26, 27]. VEI is measured vertically from the deck surface down to the steel reinforcement. Fig. 5 demonstrates how VEI measurements are accomplished. An LAE establishes an electrical connection to the steel reinforcement. Given the comparatively large size of the LAE, the impedance between the steel and LAE is negligible. The impedance of a small volume of concrete is then estimated between the center of a guarded probe and the steel reinforcement.

Factors that enhance chloride diffusion into concrete are generally correlated with the measured electrical resistance, or, conversely, electrical conductivity, of the concrete cover [24, 28]. VEI measurements identify regions of the concrete cover that have low impedance and thus indicate zones where chlorides may more easily penetrate through to the reinforcing steel. While some general parameters have been established to interpret measurements, the VEI technique lacks interpretability criteria for specific damage such as cracks.

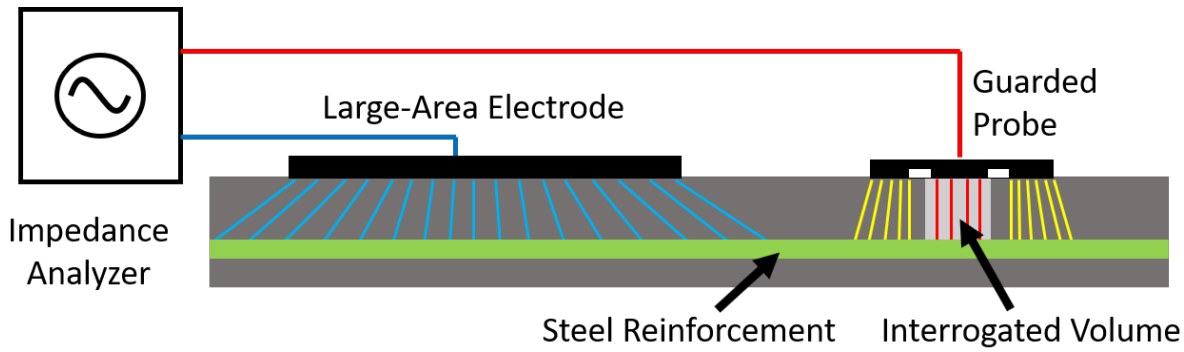

Figure 5: Schematic of vertical electrical impedance measurement technique.

This work modeled the influence of vertical cracks in the concrete cover on VEI measurements. First, some background on crack formation and electrical impedance is outlined. Second, an analytical and numerical model of VEI based on crack parameters is presented. Third, laboratory experiments validating the model are described. Fourth and finally, field experiments demonstrating the utility of the model and technique on a concrete parking garage are discussed.

2.1 Background

2.1.1 Crack Formation in Concrete Bridge Decks

Concrete cover, extending from the deck surface down to the steel reinforcement, protects the steel reinforcement from chloride ingress and accumulation [29]. Chlorides are prevalent in cold regions, where chloride-based deicing salts are routinely applied to melt ice on surfaces [30]. Chlorides are also prevalent in coastal regions due to nearby sea water [31]. As chlorides move through the protective concrete cover, they eventually reach the level of the reinforcing steel and create an environment in which the steel begins to corrode. The corrosion threshold is commonly assumed to be 1.2 kg of chloride per cubic meter [17].

Reinforcing steel corrosion is particularly hazardous for bridge decks because corroding steel expands in volume. This expansion causes significant tensile stresses in the surrounding concrete [14, 15]. Because concrete is comparatively weak in tension, continuing corrosion of the reinforcing steel typically leads to horizontal cracking known as delamination. Left untreated, the delamination will increase in size and severity, the cracking will reach the deck surface, concrete spalling will occur, and a pothole will form. Therefore, keeping bridge decks in good condition means preventing chloride ingress.

Fig. 6 shows that vertical concrete cracking causes a significant acceleration of chloride ingress towards the steel reinforcement. Surface cracks are caused by concrete shrinkage, structural deflection, vibration under loading, and thermal expansion [32]. Fig. 6 shows that vertical cracks are harmful because they provide a direct path for chlorides to penetrate the concrete cover and corrode the steel [33].

2.1.2 Electrical Impedance Techniques to Evaluate Cracks in Reinforced Concrete

The most common way that cracks in concrete are evaluated in the field is simple visual inspection. Fig. 7 a) shows the use of a crack comparator card for measuring the width of a concrete crack. This method is often used to quickly estimate the width of a crack. Automated scanning methods have also been deployed to map cracks [34,35]. Internal cracks known as delaminations, which cannot be identified visually from the surface, are investigated using a variety of nondestructive evaluation techniques, including chain drags and hammer sounding [26], automated acoustic scanning [19], infrared thermography [36], and ground penetrating radar [37].

Electrical impedance is useful as an NDT technique because it can often be rapidly deployed and is able to easily be expanded to multichannel configurations. Electrical impedance tomography (EIT) can be used to create a map of the resistivity of an object by connecting electrodes to one or more surfaces and applying voltages to one or more electrodes. Multiple configurations are iterated, and resistivity maps of the material are created by suitable inversion algorithms [38, 39].

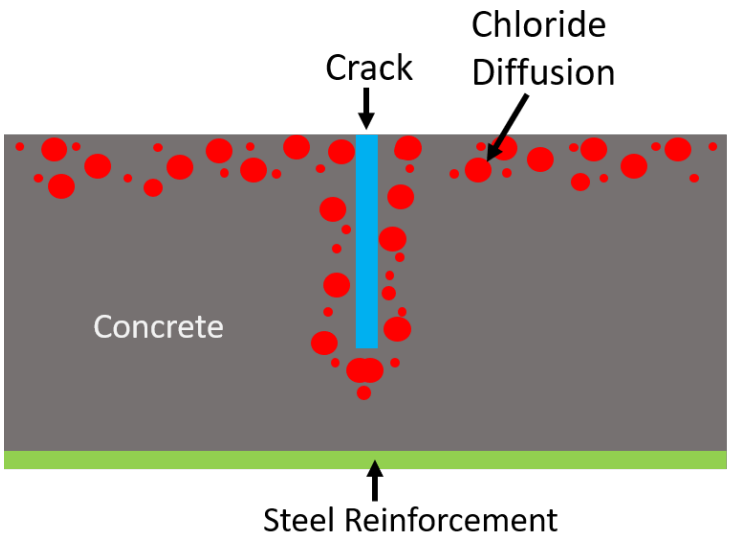

Figure 6: Cross-section of reinforced concrete with a vertical surface crack that permits faster chloride ingress.

a) b)

Figure 7: a) Photograph of a vertical crack visible on concrete deck surface and b) a cross-sectional view of damaged concrete cover with notable rebar corrosion beneath the surface.

Several studies have employed EIT, numerically and experimentally, to study cracks and other defects in materials. One study on concrete beams concluded that EIT has the ability to detect cracks and distinguish between cracks of different depths [40]. Lazarovitch et al. showed

the potential of EIT measurements to detect and localize multiple cracks in concrete [41]. Hallaji and Pour-Ghaz identified and localized damage on concrete surfaces by painting a concrete surface with a conductive paint and performing EIT on the paint [42].

Electrical impedance spectroscopy (EIS) is also used to measure concrete properties. EIS measures the impedance over a range of alternating current frequencies. EIS is primarily used as a tool to measure ion diffusion coefficients, and studies have used EIS to quantify how cracks in concrete affect the ion diffusivity of the concrete [43, 44]. Electrical impedance measurements have also been used for early-stage crack detection in steel fiber-reinforced concrete [45] and detection of cracks within concrete cylinders [46].

Many impedance studies focus on detection and localization of cracks. However, many of these techniques cannot be deployed efficiently in the field. Because VEI offers the ability to scan entire bridge decks without significant traffic disruption, even though its resolution may not favorably compare with certain tomographic techniques, inverting VEI data may be an attractive method to estimate crack parameters.

From the perspective of VEI testing, a vertical crack filled with water is essentially a region of high conductivity that has vertical orientation perpendicular to the surface of the crack. This interpretation of surface cracks reveals why, to date, VEI testing is capable of qualitatively identifying concrete cracking. After developing an understanding of how crack parameters affected VEI, this work enabled quantitative estimation of crack parameters from VEI measurements.

2.2 Analytical Model

A parameterized analytical model of VEI measurements on cracked concrete that can invert VEI data to estimate crack parameters in the field was developed in this research. Parameters include crack depth, d, crack width, w, concrete resistivity, ρ, concrete cover depth, h, and surface area over which the impedance is measured, a. These parameters are illustrated in Fig. 8.

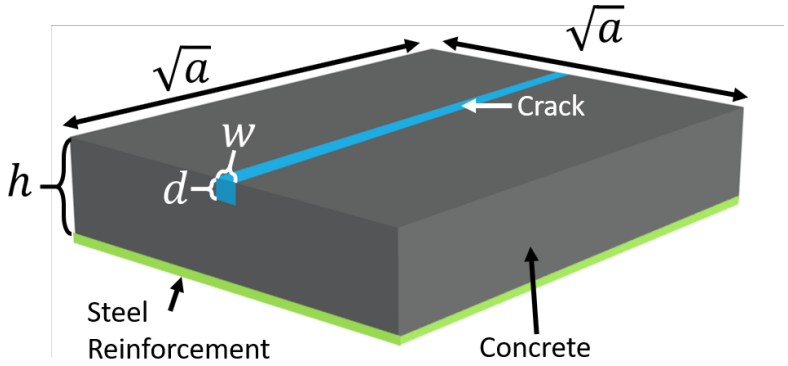

Figure 8: Analytical geometry of block and crack centered on the block.

In field measurements, the concrete deck is much larger than the probe area. A specific surface area could be identified because VEI probes are designed with a guard ring to confine the measurement region [47]. In the model, a is assumed to be the effective measurement area under the VEI probe. Although the analytical model did not require a to be square, a was assumed to be a square shape in this study. This assumption permitted intuitive geometric comparisons and was compatible with the laboratory experiments performed on square concrete slabs in this study.

2.2.1 Development of Cylinder Dipole Model

A mirrored cylinder dipole across a ground plane was used as the model basis. Similarities in current flow from a point source in a dipole and the current flow from a crack tip justified this selection. Cylinder width represented crack width, and cylinder length represented crack length.

The cylinder arrangement was analyzed using the method of images. Fig. 9 depicts the layout of this cylinder arrangement. Cylinders of radius r had centers located a distance d_{cp} from the reflection plane and had opposite charge densities of λ.

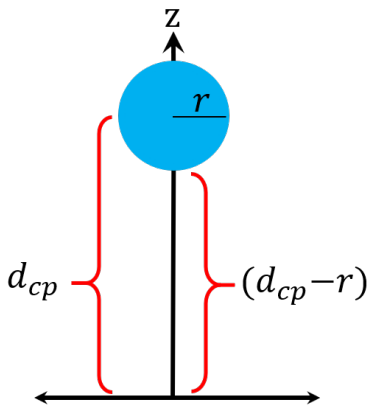

Figure 9: Layout of cylinder dipole.

In consideration of the top half of the cylinder dipole, the electric field, E, at the radius of the cylinder is given by Gauss' Law,

$$E = \frac{\lambda}{2\pi\varepsilon r}, \tag{1}$$

where ε is the permittivity of concrete and λ is the charge density on the cylinder. Electric current, I, is calculated by

$$I = \frac{2\pi r E}{\rho} \tag{2}$$

where ρ is the concrete resistivity. The charge density was unknown and needed to be determined by considering the known potential across the z-axis from $z = d_{cp} - r$ to $z = 0$. This potential, V, was described in terms of the electric field by integrating the electric field from $z = 0$ to $z = d_{cp} - r$,

$$V = \int_0^{d_{cp}-r} \frac{\lambda}{2\pi\varepsilon(d_{cp}-z)} + \frac{\lambda}{2\pi\varepsilon(d_{cp}+z)}\, dz \tag{3}$$

$$= \frac{\lambda}{2\pi\varepsilon} \ln\left(\frac{2d_{cp}-r}{r}\right). \tag{4}$$

Since V was known, the charge density was written as

$$\lambda = \frac{2\pi\varepsilon V}{\ln\left(\frac{2d_{cp}-r}{r}\right)}. \tag{5}$$

Eq. 5 was substituted into Eq. 1 to solve for E as

$$E = \frac{V}{\mathrm{r}\ln\left(\frac{2d_{cp}-r}{r}\right)}. \tag{6}$$

Eq. 6 was substituted into Eq. 2 to solve for I as

$$I = \frac{2\pi r V}{\rho\, \mathrm{r}\ln\left(\frac{2d_{cp}-r}{r}\right)}. \tag{7}$$

Finally, since the resistance was $R = \frac{V}{I}$, V could be divided by Eq. 7 to solve for the resistance between the cylinder shell and the reflection plane as

$$R = \frac{\rho}{2\pi} \ln\left(\frac{2d_{cp}-r}{r}\right). \quad (8)$$

2.2.2 From Cylinder Dipole Model to Cracked Concrete Model

Fig. 10 illustrates the comparison between the cylinder model and a cracked material. The concrete crack was modeled as a vertically-oriented rectangle and assumed to be a perfect conductor.

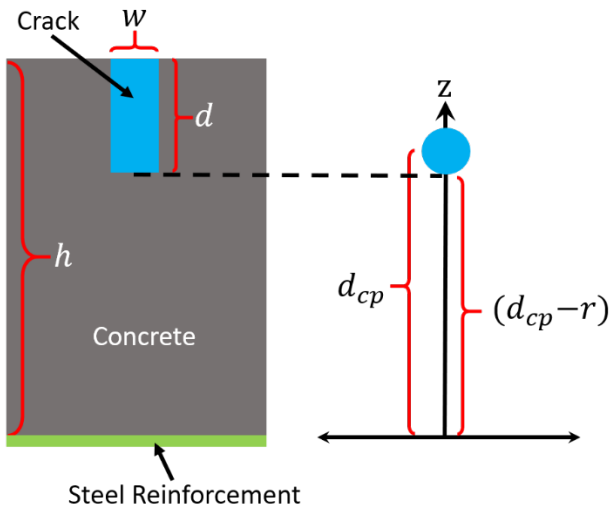

Figure 10: Comparison of cylinder dipole geometry and cracked concrete geometry.

Eq. 8 represented the resistance of the cylinder dipole model. Since presenting the analytical model in terms of cracked concrete parameters was desired, the cylinder dipole parameters in Eq. 8 were substituted for their correlated cracked concrete parameters in Eq. 9. Figs. 9 and 10 showed that $r = ½\ w$ and that $d_{cp} = (h - d) + ½\ w$. Substituting these into Eq. 8, along with some algebraic manipulation, allowed calculation of an expression for the resistance as:

$$R = \frac{\rho}{2\pi} \ln\left(\frac{4(h-d)}{w} + 1\right). \quad (9)$$

Eq. 9 calculated the resistance experienced by an electrical current moving from the cylinder shell to the reflection plane through a material with resistivity ρ. With the crack parameters now substituted into the equation, the geometry could be thought of as a block, rather than a cylinder, of cracked concrete as shown in Fig. 8.

Behavior at $d = h$ and at $d = 0$ was examined to evaluate the model. At $d = h$, the crack traveled through the whole block, creating a short circuit through the concrete block. The model correctly predicts zero impedance. When $d = 0$, a crack does not exist, indicating that the concrete is a solid block of material. Therefore, at $d = 0$, the model predicted impedance of $R_{max} = \rho h/a$. Substituting equation $d = 0$ into Eq. 9 yielded

$$R = \frac{\rho}{2\pi} \ln\left(\frac{4h}{w} + 1\right). \quad (10)$$

Eq. 9 was modified through multiplication by a scaling factor, α, such that, at $d = 0$, $R = R_{max}$. This modification was shown as

$$R_{max} = \frac{\rho h}{a} = \alpha \frac{\rho}{2\pi} \ln\left(\frac{4h}{w} + 1\right). \quad (11)$$

Solving for α yielded

$$\alpha = \frac{2\pi h}{a \ln\left(\frac{4h}{w}+1\right)}. \quad (12)$$

Multiplying Eq. 11 by Eq. 12 and simplifying yielded

$$R = \frac{\rho h}{a} \frac{\ln\left(\frac{4(h-d)}{w}+1\right)}{\ln\left(\frac{4h}{w}+1\right)} = R_{max} \frac{\ln\left(\frac{4(h-d)}{w}+1\right)}{\ln\left(\frac{4h}{w}+1\right)}. \quad (13)$$

Eq. 13 was the final analytical model used to characterize the impedance response of cracked concrete and was also invertible to estimate d. Section 2.3 provides validation of this model through numerical simulations.

2.3 Numerical Model

Numerical modeling was used to validate the analytical model and to explore the sensitivity of the model to various geometrical and material assumptions. ANSYS Electronics Desktop 2019 R3 was used to perform the numerical simulations in this work. Fig. 11 shows the 3D geometry of the concrete with an idealized crack.

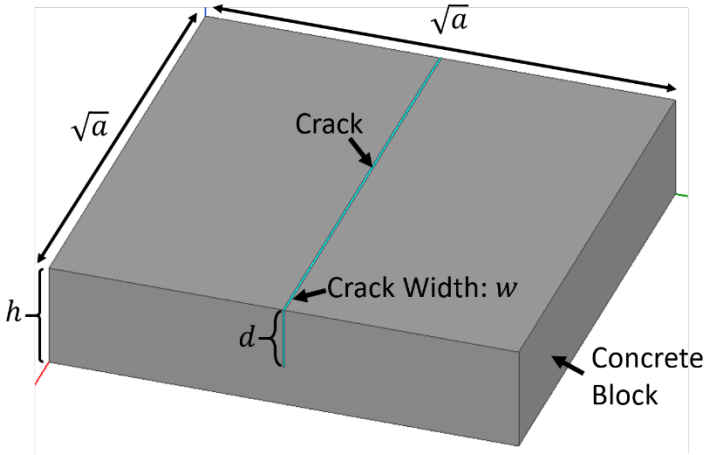

Figure 11: ANSYS model depicting simulation geometry of block and crack centered on the block.

The 3D model comprised two materials, including the concrete block and the crack. Water content greatly influences concrete resistivity. Water-saturated concrete has a resistivity of about 10^2 Ω-m, while dry concrete has a resistivity of about 10^6 Ω-m [6, 48-50]. Several values within this range were explored through numerical simulations.

Cracks are effectively empty voids. During VEI measurements, the concrete was sprayed with a conductive liquid (usually water with significant unfiltered mineral content) intended to form a good electrical contact between the VEI probe and the concrete surface but that also filled small cracks. In these simulations the resistivity of cracks was set to be 20 Ω-m, which is the resistivity of unfiltered water typically used in the laboratory and field. When the size of the block was changed, the length of the crack was also changed so that it always extended across the entire block.

2.3.1 Validation of Analytical Model

To validate the analytical model, a sensitivity analysis was performed in which the parameters were varied in the model to observe how parameter changes affected VEI. Simulation results were compared against the analytical model (Eq. 13) to estimate prediction error.

The simulations involved varying d from zero to h in regular steps and recording the simulated impedance. All other parameters were held at default values typical of concrete bridge decks and current VEI apparatus except for the varied parameter. Table 1 indicates the default values for the parameters as well as lower and upper values tested. Two sets of simulations were performed. The first varied geometric parameters of the cracks, while the second varied the material properties of the concrete and cracks while holding the geometric parameters constant.

Fig. 12 a) to f) shows the results of the simulations. The simulated impedance was normalized by the theoretical impedance value of an uncracked block, R/R_{max}, where $R_{max} = \rho h/a$ as defined previously. Normalization made comparison easier.

Fig. 12 a) to b) show the results of varying surface area, a. The results indicated that VEI could be predicted with less than 10% error for crack depths that ranged from 0% to about 90%

of the total cover depth. Fig. 12 a) to b) indicate that analytical prediction accuracy increased when the ratio of probe length to height was smaller.

Table 1: Parameter Ranges for Numerical Simulations of Cracked Concrete Blocks.

Parameter	Default value	Lower range	Upper range
a	500 cm^2	250 cm^2	1000 cm^2
w	1 mm	0.2 mm	2 mm
h	50 mm	25 mm	100 mm
$\rho_{concrete}$	10^6 Ω-m	10^2 Ω-m	10^6 Ω-m
ρ_{crack}	20 Ω-m	0 Ω-m	10^5 Ω-m

Fig. 12 c) to d) show the results of varying crack width, w. Again, the results indicated that VEI could be predicted with less than 10% error for crack depths up to 90% of the cover depth. The prediction error was smaller for larger ratios of h/w. As demonstrated in Fig. 12 c), changes in crack width w produced fairly small changes in impedance, indicating that crack width only slightly affected the impedance response. Depth appeared to much more significantly affect impedance.

Fig. 12 e) to f) shows the results of varying cover depth, h. As cover depth increased, the curvature of the analytical model increased while the curvature of the numerical model decreased. A ratio of cover depth to probe side length of about 4.4 resulted in an error below 10% for crack depths that ranged from 0% to 90% of the total cover depth. However, ratios of cover depth to probe side length of about 8.9 and 2.2 yielded analytical predictions with a poor fit to the numerical modeling. Therefore, selection of probe size must be carefully considered for specific cover depth ranges to ensure accurate analytical model predictions.

In general, the simple analytical model did well at predicting impedance over a range of common VEI measurement conditions. Additionally, some indication was given where deviations from the analytical model could be significant when cover depths were very shallow or deep.

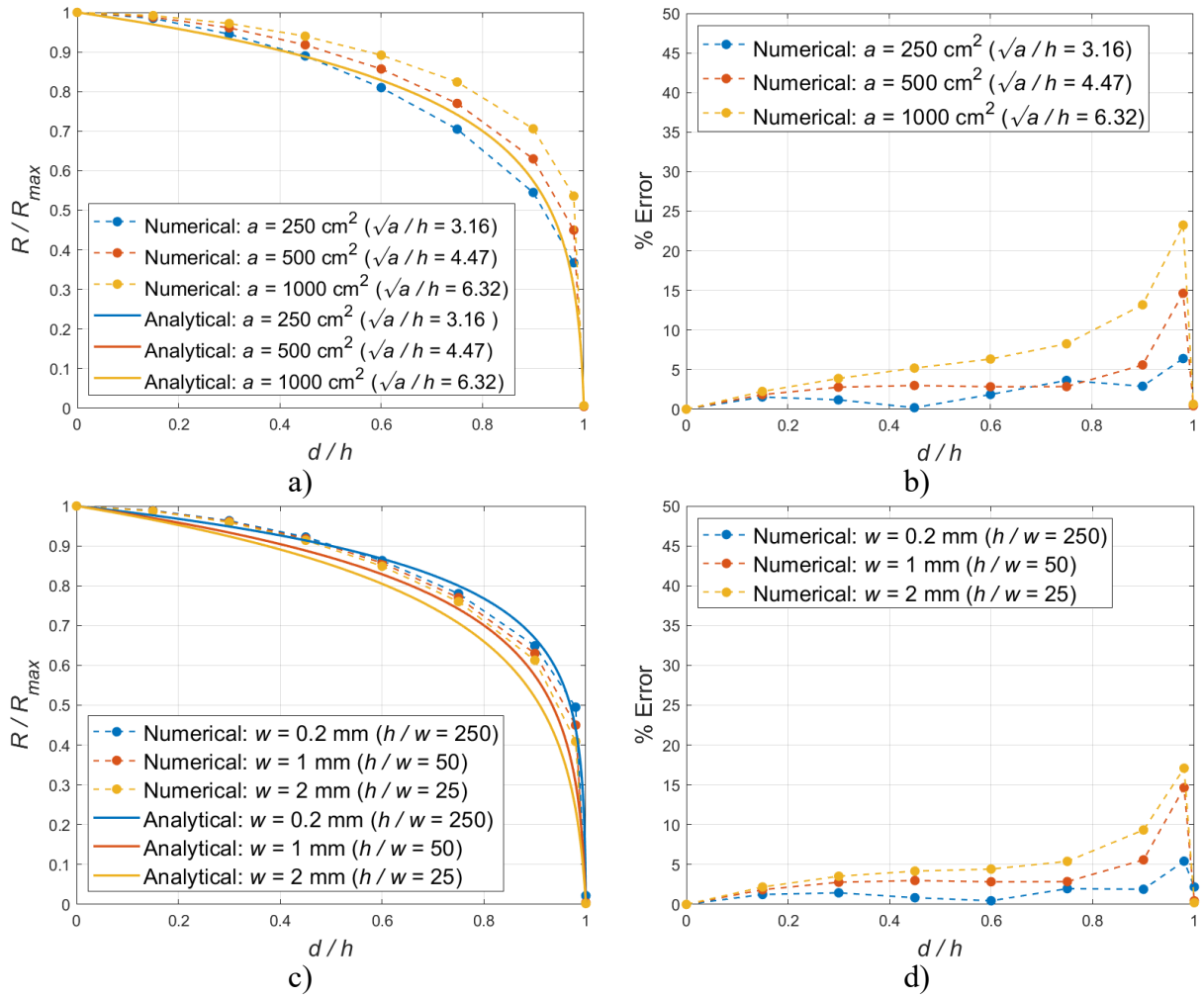

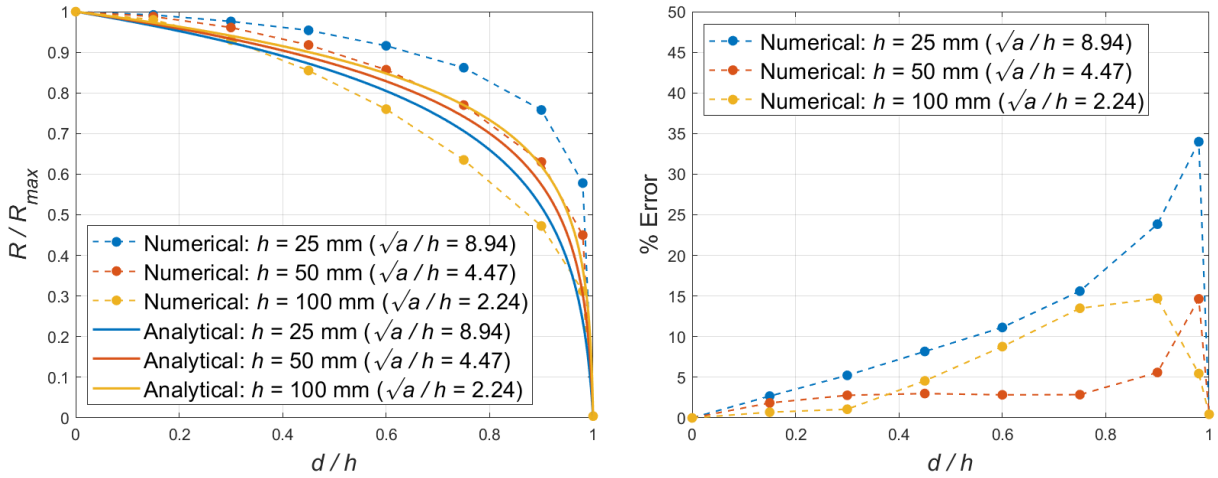

e) f)

Figure 12: Analytical model prediction compared against numerical simulations: (a) variation of effective probe area, (b) predicted error for (a), (c) variation of crack width, (d) predicted error for (c), (e) variation of cover depth, and (f) predicted error for (e).

2.3.2 Resistivity Ratio

Material changes influence the impedance. The resistivity ratio, ρ_r, was defined by

$$\rho_r = \frac{\rho_{concrete}}{\rho_{crack}}. \tag{15}$$

This ratio determines the proportion of current flowing through the crack as opposed to the surrounding concrete. As noted earlier, water-saturated concrete has a resistivity of about 10^2 Ω-m, and dry concrete has a resistivity of about 10^6 Ω-m. Fig. 13 a) displays the numerical VEI responses for wet and dry concrete. As ρ_r increased, the change in the VEI response asymptotically converged. Notably, the VEI response of $\rho_r = 10^4$ was practically indistinguishable from $\rho_r = \infty$. That is, the difference between wet and dry concrete was indistinguishable. As expected from the model and simple scaling, the resistivity ratio determined the overall response.

Fig. 13 a) also shows the analytical model. When the resistivity ratio $\rho_r \geq 10^3$, the analytical model fit the numerical simulation data with less than 10% error for crack depths that ranged from 0% to 90% of the total cover depth. The simulated data recommend a resistivity ratio of $\rho_r \geq 10^3$, which is commonly met by typical material properties of tap water and common concrete.

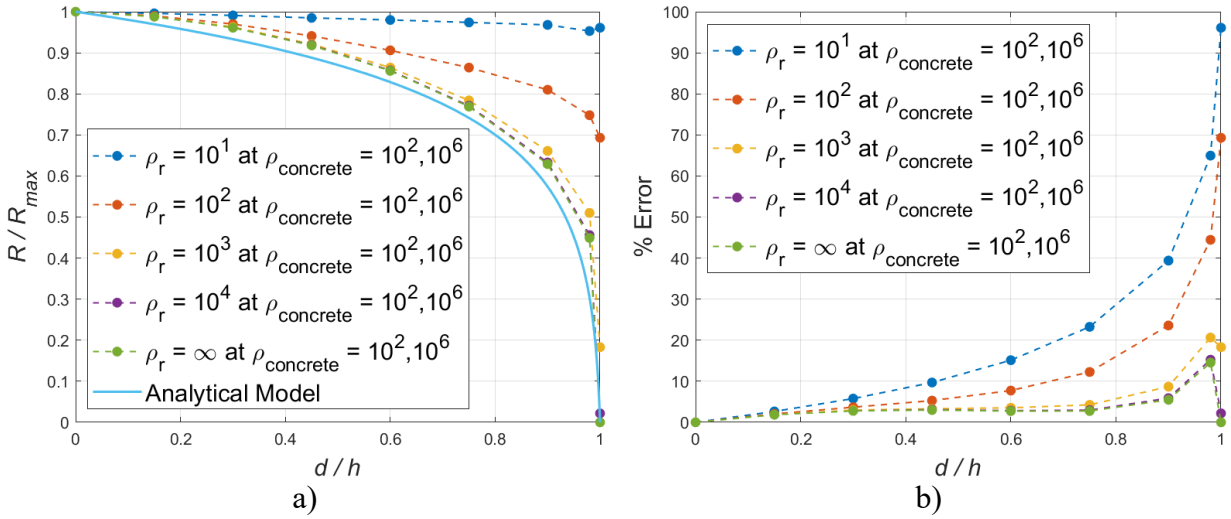

Figure 13: (a) Numerical vertical electrical impedance responses at differing ρ_r values for dry and wet concrete compared against analytical model and (b) predicted error for (a).

2.4 Laboratory Experiment

A laboratory experiment was designed to validate both the analytical and numerical models. Materials were selected to model a resistivity ratio representative of the field and to remain stable during the experiment.

Field VEI testing included spraying water over dry concrete, followed by prompt VEI measurements. This practice resulted in a resistivity ratio of about $\rho_r = 10^6\,\Omega\text{-m} / 20\,\Omega\text{-m} =$

$5x10^4$. As discussed in the previous section, when ρ_r is larger than 10^3 Ω-m, less than 10% deviation from the VEI response at $\rho_r = \infty$ occurs. Using resistivity ratios larger than $5x10^4$ was therefore appropriate for representative laboratory VEI testing.

Fig. 14 shows how this experiment was conducted. Water-saturated concrete with a thin copper mesh simulating a crack were selected. These materials have a resistivity ratio of approximately $\rho_r = 10^2$ Ω-m / 10^{-8} Ω-m $= 10^{10}$. Water-saturated concrete eliminated the variability and inhomogeneity that inevitably happens as dry concrete is wetted or wet concrete dries. Copper mesh was used as the crack simulant. To vary the crack depth in these experiments, the original concrete block was cut into two equal pieces. Water would not pool reliably within the crack. Instead, the mesh acted as a low-conductivity representation of a continuous water sheet connecting the different parts of the crack.

Fig. 14 and Fig. 15 show how the experiment was conducted. Two concrete blocks (22.86 cm by 22.86 cm by 8 cm) were pressed together with a thin mesh of copper inserted between them at a specified depth. The blocks were placed on a copper mesh that acted as a bottom electrode representing the reinforcing steel beneath the concrete cover. An Agilent 4294A Impedance Analyzer was connected to the bottom mesh and a top copper mesh. To ensure a stable electrical connection to the concrete, two concrete blocks were placed on top of the stack. These laboratory VEI measurements did not require the use of an LAE because of the direct connection to the bottom electrode.

a) b)

Figure 14: (a) Photograph of two concrete blocks used in laboratory experiment and (b) copper mesh between the concrete blocks to simulate a water-filled crack.

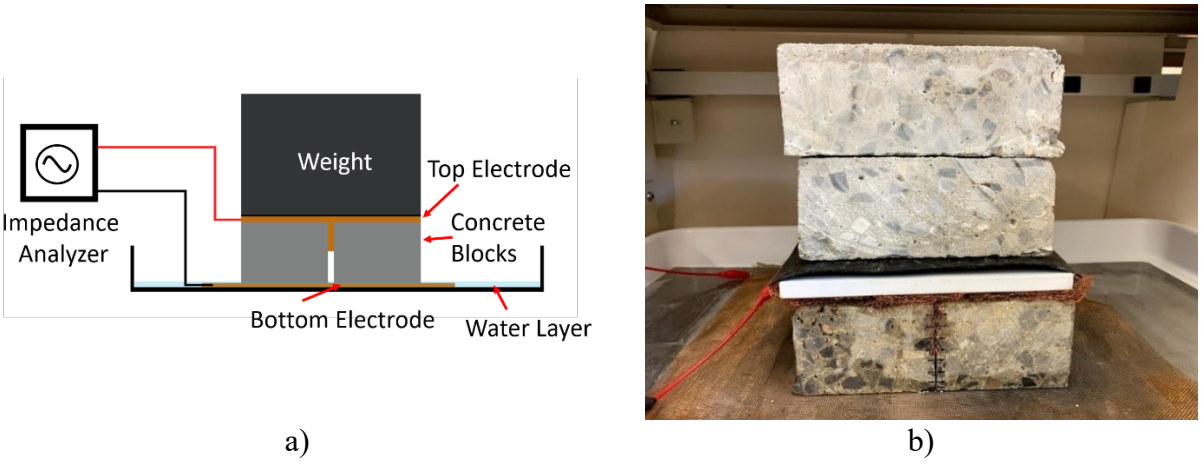

a) b)

Figure 15: a) Schematic of experiment and b) photograph of experiment.

The analyzer was set to 200 Hz with oscillator strength of 0.5 V. Starting from a depth of zero and removing and replacing the copper mesh each time, all tests were repeated five times. Experimental results are plotted in Fig. 16. The analytical prediction and numerical results from

simulations are also plotted. The maximum impedance used in the numerical simulations and the analytical model was calculated from the average impedance measurement at zero crack depth.

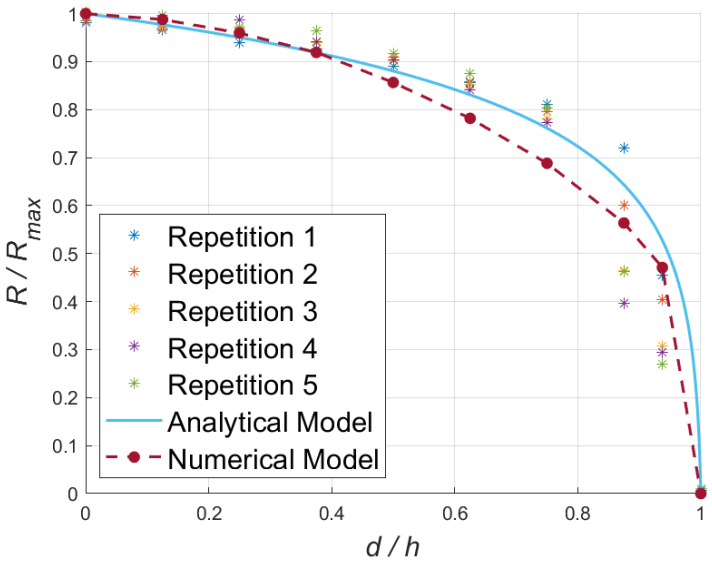

Figure 16: Saturated concrete with copper mesh crack.

The close agreement between the laboratory experimental data and the models is notable in Fig. 16, with variation increasing as the crack deepens. Some variation was due to the rough nature of the thin material at the base of the crack, creating variability. One would not expect that natural cracks in the field would have the perfect geometry of the model, so the relative agreement is a promising demonstration that the general trend is captured by the model.

The copper-type cracks with saturated concrete represent a large resistivity ratio. While this condition may not be exactly represented in the field, this experimental result gives confidence that the model can be used to interpret field results.

2.5 Field Experiments

2.5.1 Inversion of Vertical Electrical Impedance Data

Field experiments were performed to evaluate the ability of the analytical model to perform data inversion to estimate crack parameters that were difficult to measure. An important parameter is crack depth. In practice, measuring crack depth directly usually involves time-consuming, destructive drilling or coring. The inverted analytical model could thus estimate crack depth with nondestructive measurements of other parameters.

To perform inversion, Eq. 13 was used for crack depth, d. This yielded the equation

$$d = h - \frac{w}{4}\left[\exp\left(\frac{R_c a}{h\rho}\ln\left(\frac{4h}{w}+1\right)\right)-1\right]. \quad (14)$$

R_c is the VEI of the cracked portion of concrete. Concrete resistivity, ρ, was calculated by measuring the VEI of nearby intact concrete, R_i, and substituting this value into $\rho = (R_i\ a)\ /\ h$. Given these experimentally determined values, Eq. 14 simplified to

$$d = h - \frac{w}{4}\left[\exp\left(\frac{R_c}{R_i}\ln\left(\frac{4h}{w}+1\right)\right)-1\right]. \quad (15)$$

Eq. 15 indicates that crack depth can be estimated from knowledge of cover depth, crack width, VEI of the cracked section of concrete, and VEI of a nearby, intact section of concrete.

Field experiments were conducted to test the predictive ability of this model through comparison against actual measured crack depths taken with destructive measurements. A 28-year-old Salt Lake City airport parking structure that was scheduled for demolition provided a unique opportunity to test the predictions as well as perform destructive testing to determine ground truth.

2.5.2 Selection of Locations

Eight field cracks were selected and measured with nondestructive and destructive techniques. Because the concrete comprising the structure was in relatively good condition, different locations on different levels of the parking garage were necessarily selected to provide a variety of different crack types. One selected site was the east helix used for moving traffic between parking levels, where three cracks were selected for comparison. The other site was the entrance ramp at the southeast corner of the parking deck, where five cracks were selected for comparison.

2.5.3 Nondestructive Measurements

At all eight crack sites, the crack parameters necessary for crack depth prediction were nondestructively measured. As displayed in Fig. 7 a), crack width was measured visually using a standard crack comparator card. Cover depth was measured with a cover meter (Elcometer SN JK 34424-005). The impedance of both the cracked concrete and nearby intact concrete was estimated using VEI measurement equipment. VEI measurements on the helix were obtained using a single probe, while VEI measurements on the entrance ramp were selected from a scan of the entire ramp.

2.5.4 Destructive Measurements

Fig. 18 presents some of the equipment used for destructively estimating crack depth using successively smaller drill bits after the nondestructive tests were complete. Drilling was performed in 2.5-cm depth intervals through the crack. After a given lift was drilled and the powder was vacuumed, the bottom of the hole was inspected for a crack. If the crack was still

visible inside the hole, the next depth interval was drilled. This process was repeated until the crack was no longer visible.

2.5.5 Results and Discussion

Fig. 17 plots the predicted crack depths against the actual crack depths as estimated using destructive testing. H1 to H3 indicate the three samples taken on the helix, while R1 to R5 indicate the five samples taken from the entrance ramp. Upper and lower bounds of uncertainty were estimated for each sample. Due to the incremental drilling and inspecting nature of the destructive test, the measured crack depths were accurate to within approximately 2.5 cm.

Bounds on predicted values were determined by choosing ranges of values and calculating via Eq. 15. The smallest prediction formed the lower bound, and the largest prediction formed the upper bound. Samples H1, H2, H3, R2, and R3 had prediction ranges that overlapped the measured range, while samples R1, R4, and R5 had prediction ranges that did not overlap the measured range.

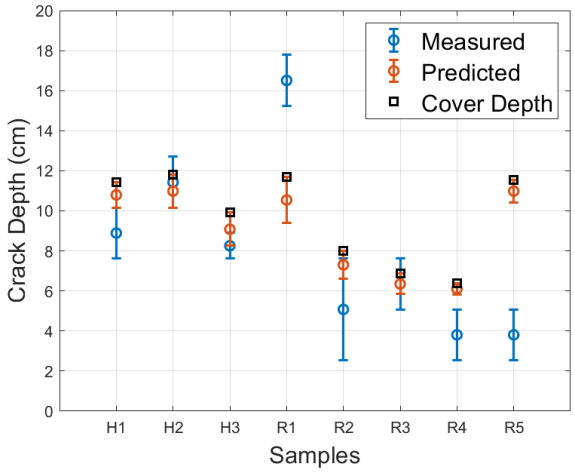

Figure 17: Measured crack depth, predicted crack depths and estimated cover depth for eight cracks in the parking structure.

For sample R1, the measured crack depth was much deeper than the predicted crack depth. In fact, the measured crack depth was several centimeters deeper than the concrete cover over the first mat of steel reinforcement. The VEI model was designed to consider only the concrete above the first mat of rebar. Thus, the deepest crack the model can predict is the full depth of the cover, h. The maximum prediction for R1 was substantially equal to the cover depth. In any case, this result indicates that the concrete cover is not protecting the steel reinforcement from chloride ingress at all.

For sample R4, the prediction was also outside the measured range. Destructive drilling to measure the crack depth was performed on the crack about 30 cm away from where the impedance was measured. As cracks do not have a uniform depth, the crack depth was likely different at the location where it was destructively measured. The difference could reasonably account for the slight differences between measured crack depth and predicted crack depth.

Figure 18: Photograph of region of concrete around sample hole R5 showing surrounding cracks as well as equipment used to make destructive measurements.

For sample R5, the predicted crack depth was deeper than the measured value. In this case, many cracks were tightly clustered together. Fig. 18 indicates where the R5 crack sample was destructively measured to estimate crack depth. As shown in Fig. 18, several other cracks were nearby. Because of the close proximity of other cracks, the VEI measurement was measuring multiple cracks at the same time, effectively in parallel, resulting in a predicted crack measurement deeper than the actual crack that was measured. Because of the damage in this area, some of the nearby cracks under the probe or other parts of this crack were probably deeper and caused the prediction to be deeper than the measurement.

Despite the difficulty in establishing ground truth for these cracks, these field experiments demonstrate that the model can be inverted to achieve success in many circumstances. However, as demonstrated by the exceptions, other factors need to be considered when interpreting VEI measurements of cracked concrete in the field.

2.6 Conclusion

This study presented a model for the quantitative influence of vertical cracks on VEI measurements. An analytical equation based on a mirrored cylindrical dipole was validated using numerical simulations and laboratory experiments. The model is particularly sensitive to the cover depth and the resistivity ratio of the concrete and the crack. Comparing the model results with numerical simulations provided insight into sizing of VEI probe area in order to optimize accuracy of model predictions. The analytical model can be inverted to predict actual crack depths measured in the field.

A limitation of the presented experiments and inversion is the possibility that the geometry of an actual crack can be highly variable and may therefore not conform closely to the

assumptions made in this study. For example, cracks may not propagate vertically, and they may be characterized by a degree of tortuosity in instances when cracking occurs around, rather than through, aggregate particles in concrete. Even with this limitation, however, this procedure enables the depth of cracks in concrete to be predicted using only NDT methods, which is a significant benefit in situations where the model can be applied.

As the VEI testing methodology increases in use and application, further work to increase the interpretability of VEI measurements, especially fusing data with other NDT methods [51], will be important. Such advances will enable those with responsibility for infrastructure management to make better decisions and apply resources in a cost-effective manner that enhances utility and safety.

CHAPTER 3. NONDESTRUCTIVE EVALUATION OF A NEW CONCRETE BRIDGE DECK SUBJECT TO EXCESSIVE RAINFALL DURING CONSTRUCTION: IMPLICATIONS FOR DURABILITY IN A COLD REGION

The contents of this chapter were prepared, submitted, and accepted as a conference paper in the Proceedings of the 2021 Regional Conference on Permafrost and 19th International Conference on Cold Region Engineering [52]. As indicated, the focus of the paper was the nondestructive evaluation of a new concrete bridge deck subject to excessive rainfall during construction.

3.1 Introduction

Nondestructive evaluation (NDE) has been extensively used to inform decisions about repair and rehabilitation of existing transportation infrastructure [53]. NDE can also be a valuable resource to provide quality assurance before acceptance of new infrastructure. In this study, NDE was used to evaluate a newly constructed concrete bridge deck in northern Utah. The durability of the bridge deck was potentially affected by an unexpected rainstorm during concrete placement. Because excess water can lead to reduced strength and/or increased permeability of concrete [54, 55], evaluation of the deck was important. Specifically, given that chloride-induced corrosion of the top mat of reinforcing steel is the leading cause of deck

damage in northern Utah as a result of routine deicing salt applications during winter maintenance [56], evaluating the ability of water and chloride ions to penetrate the concrete and quantifying the overall protection of the reinforcing steel were important objectives. The following sections provide background information, explain the procedures, present the results, and offer conclusions.

3.2 Background

The scope of this work was necessarily limited to nondestructive testing to preserve the condition of the bridge deck. To evaluate the durability of the deck, several deck properties were measured, including concrete cover depth, deck surface temperature, resistivity, VEI, and Schmidt rebound number. As described in the following sections, each method provided potentially useful information related to the objectives of the work.

3.2.1 Cover Depth

The cover depth is the distance between the nearest reinforcing steel, or rebar, and the surface of the concrete deck. Cover depth is typically estimated with an electromagnetic cover meter, which relies on the conductive properties of the steel reinforcement to produce an eddy current in response to a magnetic pulse [57]. Cover meters can accurately estimate the depth of the rebar, particularly when the diameter of the steel reinforcement is known. Cover thickness is an indication of the protection of the steel reinforcement against chloride ingress.

3.2.2 Surface Temperature

Based on inferred emissivity properties, the surface temperature of a concrete surface can be easily estimated using many readily available devices. A handheld infrared thermometer, as

used in this study, is especially useful for obtaining spot readings at locations of interest. Because chloride ion diffusivity, and hence electrical resistivity, is affected by temperature, measuring deck surface temperature can be useful if large temperature differences occur during resistivity or VEI testing, in particular.

3.2.3 Resistivity and Vertical Electrical Impedance

Both resistivity and VEI are electrical measurements designed to quantitatively assess the resistance of concrete to chloride ion penetration, where higher resistivity or impedance typically indicates reduced diffusivity of chlorides through concrete [25, 58]. Assessing the resistance to chloride ion penetration is critical in cold regions where chloride-based deicing salts are routinely applied to the deck surface during winter maintenance operations. As chloride ions diffuse through the concrete deck and accumulate in the vicinity of the rebar within the deck, steel corrosion, concrete cracking, and premature deck failure can occur [7, 56].

Traditionally, depending on the probe spacing of the testing device, resistivity measurements are used to evaluate concrete to a depth of approximately 5 cm [59], which is a typical concrete cover thickness [18]. VEI measurements, however, evaluate the total protection offered to the steel reinforcement by the full depth of the concrete cover as well as any epoxy coatings that may be present on the rebar. In a VEI test, the electrical impedance between two electrodes is measured. One of the probes is much larger than the other probe and is called the LAE [27, 48]. The LAE forms a low-resistance electrical connection to the rebar as required for the testing. Current measured through the smaller probe allows calculation of the electrical resistance between the concrete surface and the rebar.

3.2.4 Schmidt Rebound Number

A Schmidt rebound hammer can be used to estimate the compressive strength of concrete by measuring the rebound of a sprung mass after it strikes the surface of the concrete, where higher rebound numbers indicate harder, stronger concrete. When testing at a particular location is desired and surface grinding is not performed, repeated testing is warranted because crushing of the concrete matrix constituting the surface texture at that location absorbs energy that would otherwise contribute to the hammer rebound. Therefore, to ensure more representative data, only later rebound numbers are analyzed in this approach.

3.3 Procedures

The motivation for the testing performed in this research was to compare specific sections of the bridge deck, at least one of which was placed during active rain, to assess potential differences in selected concrete properties among the sections. Depicted in Fig. 19, the deck was constructed using epoxy-coated rebar, was approximately 36.5 m long and 18.3 m wide (between the parapets), and was divided into three sections that were labeled A, B, and C in order from south to north, as shown in Fig. 20 (not to scale).

The section boundaries, which are delineated by dashed lines in Fig. 20, were defined by contractor personnel. To minimize any possible bias in the evaluation, the section(s) of the deck that was placed during active rain, as well as the amount of rainfall, was not disclosed to the researchers until after the testing and analyses were complete. Within each of the three sections, a pattern comprising 10 test locations was marked for evaluation, for a total of 30 test locations.

Figure 19: Concrete bridge deck.

The bridge deck was constructed in March 2020, and the testing was performed in May 2020, almost two months later. The results of the testing are specific to the deck conditions that were prevalent during the testing period. Specifically, at the time of the testing, the deck surface was in direct sunlight and appeared to be dry, the air temperature was generally between 85 and 90°F, and wind gusts of 10 to 20 mph were typical.

As previously indicated, several deck properties were measured, including concrete cover depth, deck surface temperature, resistivity, VEI, and Schmidt rebound number. All measurements were made starting at the south end of the bridge and moving to the north end, as numbered in Fig. 20.

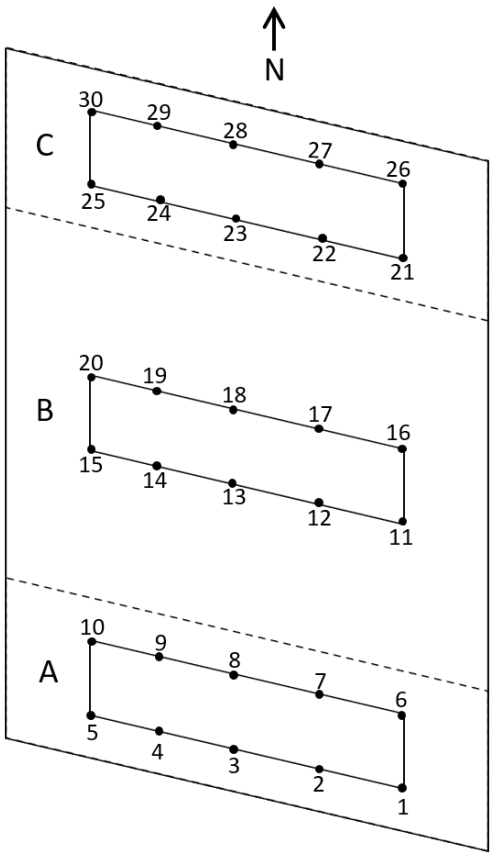

Figure 20: Test locations within sections of the bridge deck.

At each test location, the positions of the nearest longitudinal and transverse bars were determined using a cover meter and marked on the deck surface. The cover depths over those bars were then recorded. Next, the surface temperature of the concrete was measured using a spot radiometer, and then resistivity was measured using a four-prong resistivity device with a prong spacing of 5.1 cm, which was consistently oriented in the transverse direction; the prongs were always placed 5 to 8 cm away from the marked rebar. After the resistivity measurements, VEI was measured at each point. The LAE of the VEI apparatus was placed in the northwest corner of the deck, as shown in Fig. 21, where it remained for the duration of the testing. The VEI probe was connected to the LAE by a flexible wire and was moved from one test location to

the next. In order to establish a reliable electrical connection between the LAE and the deck surface, the concrete under the LAE was soaked with water and regularly re-soaked, and plastic sheeting was placed over the LAE to minimize water evaporation. In addition, the concrete at each test location was soaked with water prior to obtaining a measurement with the VEI probe. VEI measurements were recorded for at least one minute at each location. After VEI measurements were obtained and the deck surface at each test location appeared to be dry, the Schmidt hammer test was performed at each test location. The Schmidt hammer test was repeated four times at each test location, and the fourth test at each location was recorded.

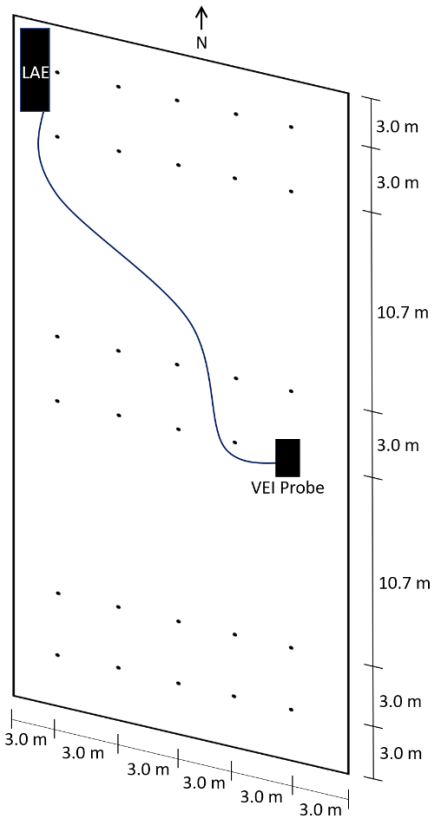

Figure 21: Location of large-area electrode and attached probe for vertical electrical impedance testing.

After data collection, an analysis of variance (ANOVA) was performed to determine if statistically significant differences were present between the three sections. An ANOVA is a method of hypothesis testing that results in a calculated probability, or *p*-value, that is compared to a threshold value for determining whether a null hypothesis can be rejected or not. If the null hypothesis can be rejected, an alternative hypothesis is accepted. In this test, the null hypothesis was that all three sections were the same, while the alternative hypothesis was that at least one section was different from another section. When the *p*-value resulting from the ANOVA was less than or equal to 0.05, which was the threshold value specified for this analysis, the null hypothesis could be rejected, and the alternative accepted; in this case, Tukey's mean separation procedure was subsequently employed to identify the specific sections that were different from each other.

3.4 Results

The results of the testing are presented in Table 1, which shows cover depth, deck surface temperature, resistivity, VEI, and Schmidt rebound number for each of the 30 test locations, where cover depth was measured over both the transverse and longitudinal reinforcing steel. Table 1 provides the average and standard deviation for each measured property for each section, while Table 2 provides corresponding *p*-values and conclusions from the ANOVA testing.

The *p*-values for four properties were less than or equal to 0.05, indicating that at least one section was different from another section with respect to those properties. Cover depths over both the transverse and longitudinal reinforcing steel were determined to be significantly different between sections B and C. Deck surface temperatures were determined to be different between sections A and C and also between sections B and C. Schmidt rebound numbers were determined to be different between sections A and C and also between sections B and C. Section

C had the highest average cover depth, the lowest deck surface temperature (it was tested last and had experienced measurable cooling from progressive changes in ambient conditions), and the lowest average Schmidt rebound number.

The *p*-values for the remaining two properties, resistivity and VEI, were both greater than 0.05, indicating that insufficient evidence existed to differentiate among the sections. Although the lowest average resistivity measurement occurred in section C, the comparatively small differences between section C and either section A or B are not statistically significant. The lowest average VEI value occurred in section A, but the comparatively small differences between section A and either section B or C are also not statistically significant. Although variations in deck temperature and/or cover depth could potentially affect resistivity and VEI, explicitly accounting for differences in these properties among the sections did not change the outcome of the analyses.

3.5 Discussion

After the testing and analyses were completed, contractor personnel explained that the concrete in section A was finished and covered prior to the onset of the rain, the concrete in section B was mostly placed but not yet covered at the time of the rain, and the concrete in section C was actively placed during the rain; 0.79 cm. of rainfall was measured at the site during the bridge deck placement. Therefore, section C was the most likely to exhibit reduced concrete strength and/or increased permeability. Several points of explanation were subsequently developed for consideration.

Table 2: Results of Data Collection

Section	Location	Cover Depth (cm)		Deck Temp.	Resistivity	VEI	Rebound Number
		Trans.	Long.	(°C)	(kΩ-cm)	(Ω)	
A	1	9.1	9.4	38.7	20.6	11700	48
	2	7.6	8.3	39.9	14.8	7200	52
	3	7.6	8.3	39.2	22.0	12000	66
	4	7.2	7.8	39.6	16.8	9800	54
	5	8.1	8.5	40.4	14.8	9300	61
	6	8.1	8.3	35.5	14.4	9300	61
	7	7.6	7.9	37.6	17.6	5000	54
	8	6.4	7.2	38.8	15.1	11750	49
	9	7.4	8.0	39.9	20.1	10750	55
	10	8.6	8.9	41.9	15.2	8600	52
Average		7.8	8.3	39.1	17.1	9540	55
St. Dev.		0.8	0.6	1.7	2.8	2217	6
B	11	7.0	7.9	39.3	15.9	15500	53
	12	5.6	6.2	38.1	19.0	18000	54
	13	7.1	7.6	36.1	13.3	9000	57
	14	6.7	7.5	35.6	18.5	8800	52
	15	7	7.8	37.7	18.4	8700	58
	16	7.1	7.8	39.0	18.3	13500	60
	17	6.6	7.1	39.2	16.0	7500	53
	18	9.5	9.8	39.0	18.0	11100	56
	19	7.2	7.6	37.7	20.5	24000	56
	20	8.0	8.5	38.7	17.9	7600	57
Average		7.2	7.8	38.0	17.6	12370	56
St. Dev.		1.0	0.9	1.3	2.0	5413	3
C	21	9.1	9.4	35.8	15.3	23000	50
	22	8.6	8.8	34.3	9.6	9700	42
	23	8.3	8.5	33.0	16.3	12500	40
	24	8.4	8.5	37.0	14.5	7800	54
	25	6.9	7.1	37.8	17.9	7000	51
	26	10.2	10.5	33.8	23.8	8500	49
	27	9.0	9.3	37.0	18.7	9400	52
	28	9.7	9.8	36.3	15.2	8800	51
	29	8.1	8.5	35.7	15.7	8250	52
	30	9.3	9.4	36.5	10.8	9000	44
Average		8.8	9.0	35.7	15.8	10395	49
St. Dev.		0.9	0.9	1.6	4.0	4663	5

Table 3: Results of Statistical Analyses

Measurement	*P*-Value	Conclusion
Cover Depth (Trans.)	0.003	B Differs from C
Cover Depth (Long.)	0.011	B Differs from C
Deck Temp.	0.000	A Differs from C B Differs from C
Resistivity	0.399	Sections Do Not Differ
VEI	0.388	Sections Do Not Differ
Rebound Number	0.002	A Differs from C B Differs from C

While some of the excess water may have been incorporated into the surface of the concrete during finishing operations, it may not have affected the full cover depth given that the resistivity test, which measures to a depth of approximately 5.1 cm, could not differentiate among the three deck sections.

The VEI testing, which measures the impedance from the deck surface to the top mat of reinforcing steel, was likely governed by the epoxy coating on the rebar. Because the concrete and the epoxy coating are in series (in terms of an electrical circuit), the one with the most resistance governs the overall result. If the epoxy coating were substantially damaged in one or more locations, the concrete would have governed in those cases. The impedance testing also could not differentiate among the three deck sections, suggesting that the reinforcing steel had consistent protection from chloride ions across all three sections.

The lower Schmidt rebound numbers in section C indicate that the concrete in section C was weaker at the surface compared to the concrete in sections A and B. However, section C also had the highest cover depth, which ensures greater protection of the reinforcing steel compared to lower cover depth, all other factors equal. Therefore, although the degree to which the higher concrete cover depth may mitigate the effects of reduced concrete strength and/or increased

permeability at the surface was not determined, the results of the testing suggest that the effect of the rain was limited to the surface of section C.

After reviewing the results of the nondestructive testing, contractor personnel arranged to investigate the depth of affected concrete through petrographic analysis of several cores removed from the bridge deck. The petrographer verified that the concrete in section A had not been affected by the rain and reported that the rain had affected only the upper 2 to 3 mm of the concrete in sections B and C, respectively. Contractor personnel then milled the deck surface to a depth of about 3 mm to remove the affected concrete and applied a 23-mm-thick polyester polymer concrete overlay, which has been demonstrated in previous research to provide excellent bridge deck protection in cold regions [30].

3.6 Conclusion

This study demonstrated the application of NDE techniques for quality assurance of a newly constructed bridge deck in northern Utah that was subjected to an unexpected rainstorm during concrete placement. To evaluate the durability of the deck, several deck properties were measured, including concrete cover depth, deck surface temperature, resistivity, VEI, and Schmidt rebound number. Statistical analyses performed on the collected data indicated that the section most affected by the rain exhibited a lower Schmidt rebound number but was not different from the other sections in terms of resistivity or VEI; therefore, the results of the testing suggest that the effect of the rain was limited to a shallow depth of concrete, which was corroborated by petrographic analysis performed on several cores removed from the bridge deck. The upper approximately 3 mm was then milled from the deck surface before a polyester polymer concrete overlay was applied to seal the deck. The techniques demonstrated in this study may be useful for assessment of other bridge decks for which evaluating the ability of

water and chloride ions to penetrate the concrete and quantifying the overall protection of the reinforcing steel are important objectives.

CHAPTER 4. CONCLUSION

The purpose of this thesis was to advance the interpretability of VEI data as gathered in concrete bridge deck inspection. The first advancement is found in Chapter 2, where an invertible analytical model for VEI measurements of cracks based on a cylindrical dipole approximation is presented. This model allows for greater understanding of how cracks affect VEI. Inversion of the model permits depth estimation of cracks and a quantitative interpretation of VEI measurements for this specific concrete defect. This is a novel contribution to scientific analysis of cracks because the geometry of cracks is so complicated that often only numerical methods are used to estimate properties. By inverting the model, crack depth can be estimated using VEI measurements. This simple inversion could be used in future studies that employ VEI testing on reinforced concrete. For example, using estimated crack depth with models of chloride diffusion to estimate remaining service life of regions of the bridge deck may prove valuable. Furthermore, this contribution is not limited to VEI measurements of bridge decks, or even concrete; this model has the potential to aid in interpreting VEI measurements of any cracked material.

The second advancement is found in Chapter 3, which highlights an application of VEI, along with several other NDT techniques, for use in quality assurance of a newly constructed bridge deck in northern Utah that was subjected to an unexpected rainstorm during concrete

placement. Comparing VEI testing with these other NDT methods has not been done before, and the results of this work will assist those who are unfamiliar with VEI with interpretation of VEI data in the context of other, more typical NDT techniques. Interpretation of VEI in terms of these traditional NDT techniques is important as it will allow the community to contextualize VEI data.

The use of VEI testing for evaluating concrete bridge decks is relatively new. Therefore, many opportunities exist for further research and development. A few topics could be explored:

1. Similar to this study, analytical models and inversion procedures could be developed to use VEI data to estimate damage in protective membranes placed under asphalt overlays that are installed on concrete bridge decks.
2. Soaking concrete with water is nonlinear and dynamic, depending on many factors. Studying the quantitative history of soaking and its effects on VEI could further inform practice and interpretation of the measurements.
3. Given the typical conditions on decks and the results of this analytical study, the probe design and size could be evaluated to best obtain and interpret VEI measurements.

VEI testing is one of several nondestructive measurements that can be used to evaluate concrete bridge decks and other structures. Advances presented in this thesis, combined with the work of many other researchers, will enable improved interpretability of VEI measurements, which will in turn enhance the utility and safety of modern infrastructure for decades to come.

REFERENCES

[1] N. Gucunski, A. Imani, F. Romero, S. Nazarian, D. Yuan, H. Wiggenhauser, P. Shokouhi, A. Taffe, and D. Kutrubes, "Nondestructive testing to identify concrete bridge deck deterioration," *Transportation research board of the national academies*, SHRP 2 Report S2-R06A-RR-1, Washington, D.C., 2013.

[2] M. C. Brown, J. P. Gomez, M. L. Hammer, and J. M. Hooks, "Long-term bridge performance high priority bridge performance issues," *Repository & open science access portal, National transportation library*, FHWA-HRT-14-052, 2014.

[3] American Road and Transportation Builders Association (ARTBA), "2020 Bridge Report," 2021.

[4] Report Card of America's Infrastructure, "Bridges," *American society of civil engineers*, 2021.

[5] B. A. Mazzeo, J. Larsen, J. McElderry, and W. S. Guthrie, "Rapid multichannel impact-echo scanning of concrete bridge decks from a continuously moving platform," *AIP conference proceedings*, Vol. 1806, p. 080003, 2017.

[6] M. Büchler, "Corrosion inhibitors for reinforced concrete," *Corrosion in reinforced Concrete Structures*, H. Böhni, Ed. Boca Raton, FL: CRC Press, pp. 190-214, 2000.

[7] J. P. Broomfield, "Corrosion of steel in concrete: understanding, investigation and repair," 2nd ed. New York, NY: *Taylor & Francis*, 2007.

[8] W. S. Guthrie and B. A. Mazzeo, "Vertical impedance testing for assessing protection from chloride-based deicing salts provided by an asphalt overlay system on a concrete bridge Deck," *Cold regions engineering*, pp. 358-369, 2015.

[9] S. Mindess, "Interfaces in Concrete," *Materials Science of Concrete, The American Ceramic Society*, 1989, pp. 163-180.

[10] P. Pullar-Strecker, I. o. C. Engineers, Ed., "Concrete Reinforcement Corrosion: From Assessment to Repair Decisions," London, England: *Thomas Telford Publishing*, 2002.

[11] S. Mindess, J. F. Young, and D. Darwin, "Concrete," *Prentice Hall*, 2003.

[12] J. H. Bungey, S. G. Millard, and M. G. Grantham, "Testing of concrete in structures," *Taylor & Francis*, 4th ed., 2006.

[13] T. M. Pinkerton, "Sensitivity of half-cell potential measurements to properties of concrete bridge decks," *Civil and environmental engineering, Ira A. Fulton college of engineering and technology*, 2007.

[14] H. Arup, "The mechanisms of the protection of steel by concrete," *Society of chemical industry*, pp. 151-157, 1983.

[15] L. Bertolini, B. Elsener, P. Pedeferri, E. Redaelli, and R. B. PolderWiley, "New book: corrosion of steel in concrete: prevention, diagnosis, repair," 2013.

[16] R. Ailaney, "Bridge preservation guide," *Federal highway administration*, 2018. [Online]. Available: https://www.fhwa.dot.gov/bridge/preservation/guide/guide.pdf

[17] J. Hema and W. S. Guthrie, "Construction and Condition Assessment of Concrete Bridge Decks and Decision Thresholds for Deck Rehabilitation and Replacement: State of the Practice," *Transportation Research Board 84th Annual Meeting Compendium of Papers, Transportation Research Board of the National Academies*, Washington, DC.

[18] J. Hema, W. S. Guthrie, and F. S. Fonseca, "Concrete bridge deck condition assessment and improvement strategies," *National transportation library*, Report UT-04-16, 2004.

[19] L. J. Hendricks, J. S. Baxter, Y. Chou, M. Thomas, E. Boekweg, W. S. Guthrie, and B. A. Mazzeo, "High-speed acoustic impact-echo sounding of concrete bridge decks," *Journal of nondestructive evaluation*, 39:58, doi:10.1007/s10921-020-00695-0

[20] R. F. Stratfull, "Half-cell potentials and the corrosion of steel in concrete," *Transportation research board*, pp. 12-21, 1973.

[21] H. Layssi, P. Ghods, A. R. Alizadeh, and M. Salehi, "Electrical resistivity of concrete," *Concrete international*, pp. 41-46, 2015.

[22] S. Hiasa, F. N. Catbas, M. Matsumoto, and K. Mitani, "Monitoring concrete bridge decks using infrared thermography with highspeed vehicles," *Structural monitoring and maintenance*, Vol. 3:3, pp. 277-296, 2016, doi:10.12989/smm.2016.3.3.277

[23] A. M. Alani, M. Aboutalebi, and G. Kilic, "Applications of ground penetrating radar (GPR) in bridge deck monitoring and assessment," *Journal of applied geophysics*, Vol. 97, pp. 45-54, 2013, doi:10.1016/j.jappgeo.2013.04.009.

[24] P. D. Bartholomew, W. S. Guthrie, and B. A. Mazzeo, "Vertical impedance measurements on concrete bridge decks for assessing susceptibility of reinforcing steel to corrosion," *Review of scientific instruments*, Vol.83: 085104, 2012.

[25] W. S. Guthrie, J. Baxter, and B. A. Mazzeo, "Vertical impedance testing of a concrete bridge deck using a rolling probe," *NDT&E International*, Vol. 95, 65-71, 2018.

[26] B. A. Mazzeo and W. S. Guthrie, "Vertical electrical impedance scanner for concrete bridge deck assessment without direct rebar attachment," *NCHRP IDEA Project 202 Final Report*, 2019.

[27] J. Baxter, L. Hendricks, W. S. Guthrie, and B. A. Mazzeo, "Instrumentation for multi-channel vertical electrical impedance scanning of concrete bridge decks," *Engineering research express*, Vol. 2: 035010, 2020.

[28] H. M. Argyle, "Sensitivity of Electrochemical Impedance Spectroscopy Measurements to Concrete Bridge Deck Properties," *BYU scholars archive,* 3963, 2014.

[29] T. W. Emery, "Development of a management guide for concrete bridge decks in Utah," *HBL Library*, 2020.

[30] S. Colson, "Evaluation of 6 modified salt spreaders," *National transportation library*, Maine, 2007.

[31] Kessler, J. Richard, Powers, G. Rodney, and I. R. Lasa, "An update on the long term use of cathodic protection of steel reinforced concrete marine structures," *Paper presented at the CORROSION 2002*, Denver, Colorado, April 2002.

[32] ACI Committee 224, "Control of Cracking of Concrete Structures," *American Concrete Institute*, ACI 224R-01, Farmington Hills, MI, 2001.

[33] A. Patnaik and P. Baah, "Cracking behavior of structural slab bridge decks," *University of Akron*, Report no. FHWA/OH-2015/4, 2015.

[34] K. Won and C. Sim, "Automated transverse crack mapping system with optical sensors and big data analytics," *Sensors (Basel),* Vol. 20(7):1838, doi:10.3390/s20071838. PMID: 32224937; PMCID: PMC7181289. 2020.

[35] J. Valença, I. Puente, and E. N. B. S. Júlio, "Assessment of cracks on concrete bridges using image processing supported by laser scanning survey," *Construction and building materials*, Vol. 146, pp. 668-678, DOI:10.1016/j.conbuildmat.2017.04.096, 2017.

[36] A. Ellenberg, A. Kontsos, F. Moon, and I. Bartolic, "Bridge deck delamination identification form unmanned aerial vehicle infrared imagery," *Automation in construction*, Vol. 72:2, pp. 155-165, 2016.

[37] K. Dinh and N. Gucunski, "Factors affecting the detectability of concrete delamination in GPR images," *Construction and building materials*, Vol. 274, 121837, 2021.

[38] T. Kriz and J. Dusek, "Electrical impedance tomography in the testing of material defects," *Conference: Progress in Electromagnetics Research Symposium - Spring (PIERS),* 2017.

[39] W. Fan, Q. Xue, H. Wang, and B. Tian, "Damage Detection in Cross-Ply CFRP Based on Open Electrical Impedance Tomography," *2016 International Conference on Information System and Artificial Intelligence* (ISAI), pp. 446-450, 2016, doi: 10.1109/ISAI.2016.0101, 2016.

[40] K. Karhunen, A. Seppanen, A. Lehikoinen, J. Blunt, J. P. Kaipio, and P. J. Monteiro, "Electrical resistance tomography for assessment of cracks in concrete," *ACI Materials Journal*, 107(5):523-531, 2010.

[41] R. Lazarovitch, D. Rittel, and I. Bucher, "Experimental crack identification using electrical impedance tomography," *NDT & E International*, Vol. 35:5, pp. 301-316, 2002.

[42] M. Hallaji and M. Pour-Ghaz, "A new sensing skin for qualitative damage detection in concrete elements: Rapid difference imaging with electrical resistance tomography," *NDT & E International*, 68:13-21, 2014.

[43] A. Akhavan and F. Rajabipour, "Evaluating ion diffusivity of cracked cement paste using electrical impedance spectroscopy," *Mater Struct 46*, pp. 697–708, 2013. https://doi.org/10.1617/s11527-012-9927-x

[44] A. Akhavan and F. Rajabipour, "Quantifying Permeability, Electrical Conductivity, and Diffusion Coefficient of Rough Parallel Plates Simulating Cracks in Concrete," *Journal of Materials in Civil Engineering*, Vol. 29:9, 2017.

[45] T. Zhang, L. Zhou, H. Ammari, and J. K. Seo, "Electrical impedance spectroscopy-based defect sensing technique in estimating cracks." *Sensors (Basel),* Vol. 15(5):10909-22. doi: 10.3390/s150510909. PMID: 26007713; PMCID: PMC4481952.

[46] M-S. Kang, Y-K. An, and D-J. Kim, "Electrical impedance-based crack detection of SFRC under varying environmental conditions," *Department of Architectural Engineering and Department of Civil and Environmental Engineering, Sejong University,* 209, Neungdong-ro, Gwangjin-gu, Seoul, 05006, Republic of Korea, 2018.

[47] D. J. Barton, J. Baxter, W. S. Guthrie, and B. A. Mazzeo, "Large-area electrode design for vertical electrical impedance scanning of concrete bridge decks," *Review of scientific instruments*, Vol. 90:2, 025101 (2019): https://doi.org/10.1063/1.5058152.

[48] G. P. Gu, J. J. Beaudoin, and V. S. Ramachandran, "Handbook of analytical techniques in concrete science and technology: principles, techniques, and applications," Park Ridge, NJ: *Noyes Publications*, 2001.

[49] V. M. Malhotra and N. J. Carino, "Handbook on Nondestructive Testing of Concrete," 2nd ed. West Conshohocken, PA: *CRC Press*, 2004.

[50] A. M. Neville, "Properties of Concrete," 3rd ed. Marshfield, MA: *Pitman Publishing*, 1981.

[51] S. Pashoutani, J. Zhu, C. Sim, K. Wan, B. A. Mazzeo, and W. S. Guthrie, "Multi-sensor data collection and fusion using deep autoencoders in condition evaluation of concrete bridge decks," *Journal of Infrastructure Preservation and Resilience*, 2021.

[52] E. Boekweg, W. S. Guthrie, and B. A. Mazzeo, "Nondestructive Evaluation of a New Concrete Bridge Deck Subject to Excessive Rainfall during Construction: Implications for Durability in a Cold Region," *American Society of Civil Engineers,* 2021 Regional Conference on Permafrost and 19th International Conference on Cold Region Engineering, 2021.

[53] W. S. Guthrie, T. Waters, J. S. Baxter, L. Hendricks, and B. A. Mazzeo, "New tools for evaluating concrete bridge decks: high-speed acoustic impact-echo and vertical electrical impedance testing of Utah's longest bridge deck," *Proceedings of the Bridge Engineering Institute Conference,* Honolulu, HI, 2019.

[54] Y. Y. Kim, K. M. Lee, J. W. Bang, and S. J. Kwon, "Effect of W/C ratio on durability and porosity in cement mortar with constant cement amount," *Advances in Material Science and Engineering*, 273460, 2014.

[55] S. Popovics and J. Ujhelyi, "Contribution to the concrete strength verses water-cement ratio relationship," *Journal of Materials in Civil Engineering*, Vol. 20:7, pp. 459-463, 2008.

[56] J. Barton, J. Baxter, W. S. Guthrie, and B. A. Mazzeo, "Vertical electrical impedance scanner for nondestructive concrete bridge deck assessment without a direct rebar connection," *Materials Evaluation,* Vol. 77:10, pp. 1258-1266, 2019b.

[57] L. Fernandez, "Non-destructive evaluation of the concrete cover: Comparative test–part II: comparative test of cover meters," *Materials and Structures*, Vol. 38:284, pp. 907-911, 2005.

[58] W. S. Guthrie, J. S. Baxter, and B. A. Mazzeo, "Vertical electrical impedance testing of a concrete bridge deck using a rolling probe," *NDT & E International*, Vol. 95, pp. 65-71, 2018.

[59] J. W. McCarter, G. Starrs, S. Kandasami, R. Jones, and C. Malcolm, "Electrode configurations for resistivity measurements on concrete," *ACI Materials Journal*, Vol. 106:3, pp. 258-264, 2009.

[60] R. J. Stevens, W. S. Guthrie, J. S. Baxter, and B. A. Mazzeo, "Field evaluation of polyester polymer concrete overlays on bridge decks using nondestructive testing," *Journal of Materials in Civil Engineering*, in press, 2020.